The phonon wake behind a charge moving relative to a two-dimensional plasma crystal

Daniel H. E. Dubin
Department of Physics, University of California at San Diego, La Jolla, California 92093

(Received 18 May 2000; accepted 14 July 2000)

In a recent experiment a wake was created in a two-dimensional lattice of charged dust grains by a charge moving parallel to the lattice plane. Multiple ''Mach cones'' were observed in the wake. This paper describes a linear theory of the phonon wake caused by a charge moving relative to a crystalline lattice. The theory predicts multiple structures in the wake that are qualitatively similar to those observed in the experiments. These structures are caused by constructive interference of compressional phonons excited by the moving charge, combined with the strongly dispersive nature of these phonons. © *2000 American Institute of Physics.* [S1070-664X(00)04810-2]

I. INTRODUCTION

The wake created by an object moving with respect to a medium is a ubiquitous phenomenon, occurring on astronomical scales (e.g., the earth's magnetotail formed by interaction with the solar wind), human scales (e.g., the shock wave behind a supersonic airplane), and microscopic scales (e.g., Cherenkov radiation created by a rapidly moving elementary charge). In some cases the dynamics of the wake is nonlinear (as in the first two examples), whereas in other cases a linear analysis suffices (as in the last example). In these (and other) examples the structure of the wake has received close scrutiny, and in some cases it is still a topic of current research.

Recently the wake created in a crystal lattice by a moving charge was observed and measured.[1,2] In condensed matter physics, the interaction of moving charges with a lattice is clearly of great significance. For example, the excitation of phonons during ion implantation is known to be an important process.[3] However, the spatial characteristics of the wake created by a moving charge in a crystal has not received much attention (to our knowledge), possibly because the spatial scales involved are typically small, and the time scales are fast (set by the atomic spacing and the sound speed, respectively). These difficulties were avoided in the aforementioned experiments, because the crystal consisted of a two-dimensional (2D) triangular lattice of charged dust grains (polymer microspheres) with large spacing, $a \simeq 250$ microns. The grains were levitated against the force of gravity in the sheath of a rf plasma discharge. A charge (another microsphere, or possibly an agglomeration of several microspheres) moving parallel to the crystal plane with nearly constant speed U of only a few cm/s perturbed the positions of the dust grains, creating a wake in the lattice that could be imaged with a digital camera.

The wake had some expected features as well as several unexplained structures. As expected, a ''Mach cone'' was observed, in which a perturbation was concentrated in a cone with opening angle β, and had an angle of propagation $\theta = \theta_0$ that obeyed the usual Mach conditions,

$$\beta = \theta_0, \quad c(0) = U \sin\theta_0, \tag{1}$$

[where $c(0)$ is the sound speed of long-wavelength phonons]. The angles θ and β are defined in Fig. 1. [The angle of propagation for a wave with wave number $\mathbf{k}$ is $\theta = \tan^{-1}(k_y/k_x)$; the angle β is defined for a given displacement (x_0, y_0) from the moving charge as $\beta = \tan^{-1}(x_0/(-)y_0)$.] Equation (1) merely prescribes that surfaces of constant phase keep pace with the moving charge, so that the driven wave can be resonant with the charge. However, several other ''Mach cones'' with different (smaller) opening angles also appeared in both experiments and simulations, and these structures were unexplained.

This paper outlines a general linear theory for the wake induced by a charge moving at constant velocity with respect to a 2D crystalline lattice. The theory should be valid at the high densities associated with regular condensed matter. When applied to a 2D dust plasma lattice, the theory predicts multiple structures in the wake that are qualitatively similar to those observed in the experiments and simulations. The multiple wake structures are a consequence of the strongly-dispersive nature of compressional phonons (sound waves) in a 2D lattice. The excited waves satisfy the Mach condition, $c = U \sin\theta$ but $c = c(\mathbf{k})$ so different excited waves travel at different propagation angles, $\theta = \theta(\mathbf{k})$. Phase mixing of the various excited waves causes constructive and destructive interference. As a result, along a line defined by some given opening angle β we will show that specific wave numbers $\mathbf{k} = \mathbf{k}_0(\beta)$ are dominant, and in general the propagation angle θ for these wave numbers is not equal to β. These wave numbers form the observed multiple wakes.

Such structures do not occur in the single Mach cone shock wave surrounding a particle in air that moves faster than the speed of sound. This is because air is much less dispersive than a 2D lattice, so Eq. (1) is nearly correct for all significant wave numbers. On the other hand, many other media have strong dispersion and therefore also exhibit multiple wake structures. Probably the best known example is the so-called ''Kelvin wedge'' that forms behind a ship moving in deep water, caused by the strong linear dispersion of deep water surface waves.[4]

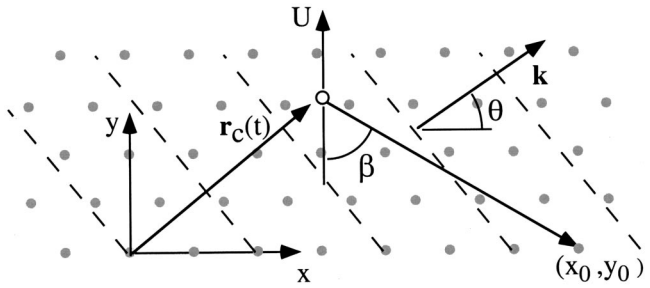

FIG. 1. A moving charge at position $\mathbf{r}_c(t)$ excites a phonon with wave number $\mathbf{k}$, propagating at angle θ with respect to the x axis. Surfaces of constant phase are shown as dashed lines. The phonon perturbs a dust grain located at position (x_0, y_0), measured with respect to the moving charge.

In a 2D crystal, the phonon wake structure depends on the speed of the moving particle, U. When $U > c(0)$, we find that there is a linear Mach cone satisfying Eq. (1) along with a secondary ''lateral'' oscillatory wake with smaller angles β and θ. In addition, there is a narrow wake due to umklapp phonons (phonons from beyond the first Brillouin zone of the lattice) that is superimposed on the lateral wake. The wave crests are displayed in Fig. 2(a). The narrow umklapp wake is sensitive to details such as the direction of motion of the charge with respect to the lattice. However, the Mach cone and the lateral wake at larger opening angles are insensitive to these details.

For $U < c(0)$ the Mach cone disappears and is replaced by a ''transverse'' oscillatory wake similar to that behind a moving ship in deep water.[4] This sort of wake is displayed in Fig. 2(b). The theory behind Figs. 2(a) and 2(b) will be the subject of the next section.

II. THEORY

Consider an infinite lattice of identical charged dust grains, with charge Q and mass m, confined to the $x-y$ plane in the sheath of a background plasma. A moving charge below the plane, with projected (x,y) position $\mathbf{r}_c(t) = x_c\hat{x} + Ut\hat{y}$ at time t, creates a force $-\nabla\Phi(\mathbf{r}_i - \mathbf{r}_c(t))$ on the ith dust grain, at position $\mathbf{r}_i$. The grains interact with one another via a Yukawa potential $\phi(|\mathbf{r}_i - \mathbf{r}_j|)$, where

$$\phi(r) = Q^2 \frac{e^{-r/\lambda}}{r}, \tag{2}$$

and where λ is the Debye screening length of the background plasma sheath. This is a good approximation for particles suspended at the same height in the plasma sheath.[5] The potential $\Phi(\mathbf{r})$ is less-well understood, since the moving charge is at a different height in the sheath than the dust grains. Some research has pointed to an attractive interaction between grains at different heights;[7–9] others have observed grain repulsion in some circumstances.[5,6] In what follows we will leave Φ an unknown function. We will soon see that the wake structure depends on Φ, and the current experimental data together with the theory imply that Φ cannot be a purely attractive potential; the force between the moving charge and the grains either changes sign or is purely repulsive.

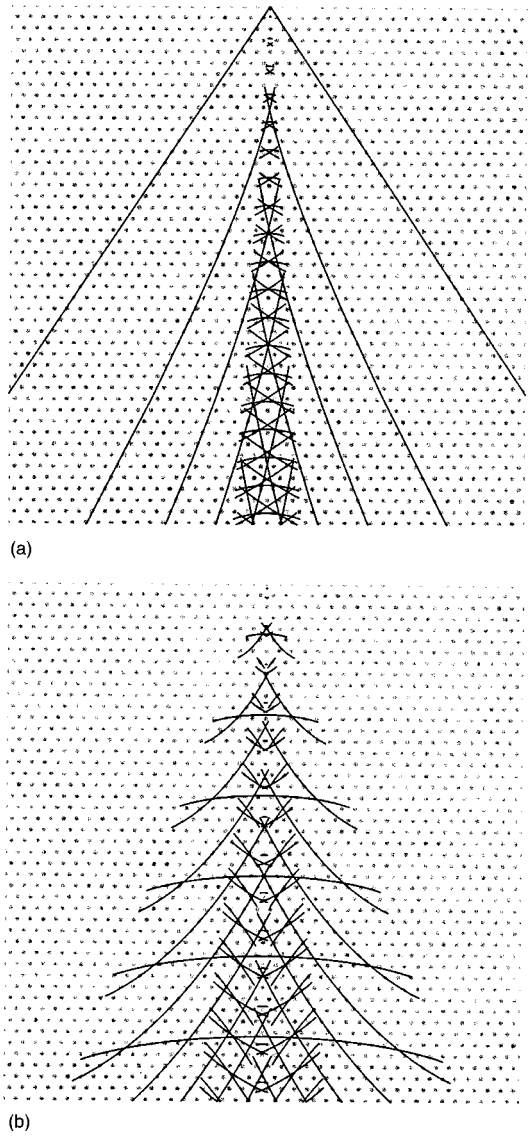

FIG. 2. Structure of the wake behind a charge moving in the positive y direction (up in the figures). Lines display wave crests; or more precisely, maxima of the function $\sin(\mathbf{k}_0(\beta)\cdot(x_0, y_0) + (\pi/4)\mathrm{sgn}(u))$, assuming a Yukawa interaction with $\lambda/a = 1$. Gray dots are the positions of charges in the triangular lattice, with spacing shown to scale with respect to the wake. (a) $U/c(0) = 1.8$; (b) $U/c(0) = 0.8$.

Assuming that the perturbed dust grain position $\delta\mathbf{r}_i$ is small, $\delta\mathbf{r}_i$ satisfies the following linearized equation of motion:

$$m\,\delta\ddot{\mathbf{r}}_i = -\nabla\Phi(\mathbf{r}_i - \mathbf{r}_c(t)) - \sum_{j\neq i} \frac{\partial^2\phi}{\partial\mathbf{r}_i\partial\mathbf{r}_i}(\mathbf{r}_i - \mathbf{r}_j) \cdot[\,\delta\mathbf{r}_i - \delta\mathbf{r}_j] - m\nu\,\delta\dot{\mathbf{r}}_i,$$

where ν is a phenomenological damping rate, caused by collisions of the grains with neutral gas. This linear equation can be solved for the driven response of the dust grains to the force of the moving charge by introducing phonon coordinates and Fourier transforming. The result of this analysis is

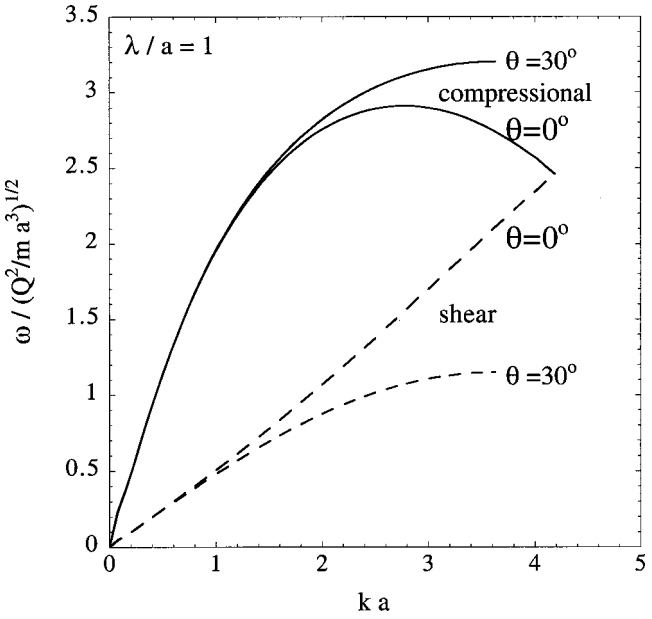

FIG. 3. Frequency ω versus wave number k in the first Brillouin zone for shear and compressional modes in a 2D triangular dust plasma lattice, for two angles of propagation with respect to the x,y axes [$\mathbf{k}=k(\cos\theta,\sin\theta)$]. The lattice is oriented as shown in Fig. 1, and the Yukawa potential with $\lambda/a=1$ is assumed.

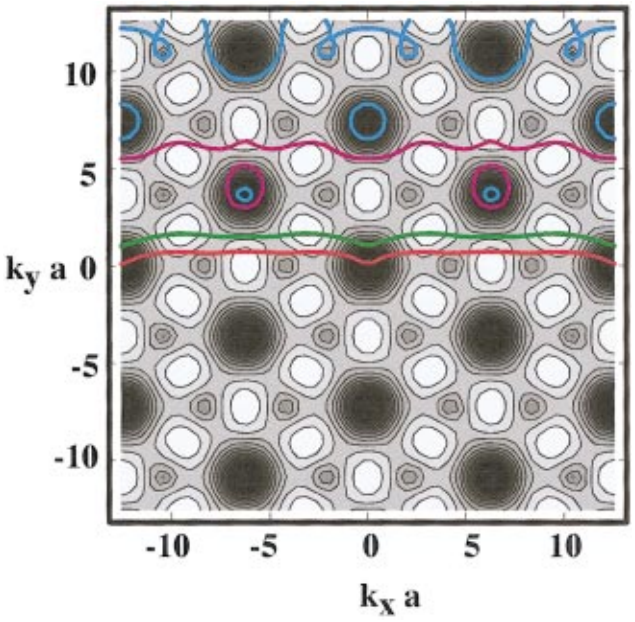

FIG. 4. (Color) Resonance curves [solutions of Eq. (5)], for $U/c(0)=1.8$ (red), 0.8 (green), 0.2 (purple), 0.1 (blue). Also shown in gray are contours of constant ω. $\lambda/a=1$ is used in the Yukawa potential, and in this case $c(0)=2.43(Q^2/ma)^{1/2}$.

$$\delta\mathbf{r}_i(t)=-\sum_\alpha \int \frac{d^2\mathbf{k}}{(2\pi)^2} \times \frac{i\hat{\Phi}(\mathbf{k})\mathbf{k}\cdot\hat{e}_\alpha(\mathbf{k})\hat{e}_\alpha(\mathbf{k})e^{i\mathbf{k}\cdot(\mathbf{r}_i-\mathbf{r}_c(t))}}{\omega_\alpha^2(\mathbf{k})-k_y^2U^2-i\nu k_yU}, \tag{3}$$

where $\hat{\Phi}(\mathbf{k})=\int d^2\mathbf{r}\Phi(\mathbf{r})e^{-i\mathbf{k}\cdot\mathbf{r}}$ is the Fourier integral of $\Phi(\mathbf{r})$ and $\omega_\alpha(\mathbf{k})$ and $\hat{e}_\alpha(\mathbf{k})$ are the frequency and polarization unit vector of a phonon with wave number $\mathbf{k}$. In the wave number integral in Eq. (3), ω_α and $\hat{e}_\alpha$ are periodic functions of $\mathbf{k}$, repeating in each Brillouin zone of the 2D triangular lattice. The subscript α denotes the type of phonon; $\omega_\alpha^2(\mathbf{k})$ and $\hat{e}_\alpha(\mathbf{k})$ are the eigenvalue and eigenvector, respectively, of a matrix $\mathbf{M}(\mathbf{k})$, where

$$\mathbf{M}(\mathbf{k})=\frac{1}{m}\sum_{j\neq i}\frac{\partial^2\phi}{\partial\mathbf{r}_i\partial\mathbf{r}_i}(\mathbf{r}_i-\mathbf{r}_j)[1-\cos\mathbf{k}\cdot(\mathbf{r}_i-\mathbf{r}_j)]. \tag{4}$$

For a 2D lattice, this matrix is 2×2, with two types of phonons, termed compressional and shear [for $ka\ll1$, $\hat{e}(\mathbf{k})\|$ or $\perp$ $\mathbf{k}$, respectively]. The frequency of the phonons in the first Brillouin zone is shown in Fig. 3 along two directions. The lattice is assumed to be oriented with respect to x and y as shown in Fig. 1. Contours of constant frequency are shown across several Brillouin zones for the compressional mode in Fig. 4. The phase velocity of the compressional phonons is larger than that of the shear branch.[1,10] The wake is therefore dominated by the compressional branch, and we will concentrate on the compressional phonons in the remainder of the paper. Some other numerical and analytic results for the compressional modes are discussed in the Appendix.

The wave number integral in Eq. (3) is dominated by the pole, at $\omega_\alpha^2=k_y^2U^2-i\nu k_yU$. Dropping the imaginary part, we denote $k_{y_0}(k_x)$ as the solution to the resonance condition

$$\omega_\alpha^2(k_x,k_{y_0})=k_{y_0}^2U^2. \tag{5}$$

Note that this resonance condition is just the Mach condition $c\equiv\omega/k=U\sin\theta$, where $\theta=\tan^{-1}(k_y/k_x)$ is the angle of propagation. Solutions of Eq. (5) for $k_{y_0}(k_x)$ for the compressional phonons are shown in Fig. 4 for several values of U, and for Debye length equal to interparticle spacing in the Yukawa potential. Only solutions with $k_{y_0}>0$ are shown, although the symmetry of the lattice implies that $-k_{y_0}(-k_x)$ is also a solution. Wave numbers beyond the first Brillouin zone correspond to umklapp phonons, and should be referred back to wave numbers in the first Brillouin zone by subtracting out a reciprocal lattice wave vector: $\mathbf{k}\to\mathbf{k}-\mathbf{g}$, where $\mathbf{g}=n(0,4\pi/\sqrt{3}a)+m(2\pi/\sqrt{3}a,2\pi/a)$, and m and n are integers.

One may observe in Fig. 4 that when $U>c(0)$, $k_{y_0}\to0$ as $k_x\to0$. This is because $\omega\approx c(0)k$ at small k, so Eq. (5) approaches Eq. (1) and $k_{y_0}=|k_x|\tan\theta_0$ as $k_x\to0$. On the other hand, for $U<c(0)$, Eq. (1) no longer has a solution, and k_{y_0} no longer approaches zero as $k_x\to0$.

In fact, for sufficiently small $U/c(0)$, one can see from Fig. 4 that k_{y_0} is no longer even in the first Brillouin zone for any k_x value. Referring such high-wave-number solutions back to the first Brillouin zone, we see that umklapp phonons are excited nearly isotropically by a slow-moving charge. However, the experiments were performed for $U>c(0)$, so we will concentrate on this case for the moment.

Returning to the evaluation of the k_y integral in Eq. (3), it is convenient to work in a coordinate frame moving with

the charge, so we define $(x_0,y_0)=\mathbf{r}_i-\mathbf{r}_c(t)$. Equation (3) shows that the wake is stationary in the moving frame. The location of the pole in the k_y integral can be found approximately assuming ν is small; $k_y\simeq k_{y_0}(k_x)-i\nu/2[U-v_{g_y}(k_x,k_{y_0}(k_x))]$, where $k_{y_0}(k_x)$ is given by Eq. (5), $\mathbf{v}_g=\partial\omega_\alpha/\partial\mathbf{k}$ is the group velocity, and $v_{g_y}=\mathbf{v}_g\cdot\hat{y}$. When $U>v_{g_y}$, the pole is in the lower-half plane. Keeping only the contribution from this pole in the k_y integral of Eq. (3), the result is nonzero only for $y_0=y-Ut<0$. Otherwise, if $y_0>0$ the k_y contour of integration must be closed in the upper half-plane, where there are no poles. Thus, when $U>v_{g_y}(k_x,k_{y_0})$ the wake trails the moving charge; but the same argument implies that if $U<v_{g_y}(k_x,k_{y_0})$ the wake is in front of the charge.

Note that in the experiments of Refs. 1 and 2, $U>c(0)$, and for compressional modes $c(0)>|\mathbf{v}_g|$ (see Fig. 3), so the above argument implies that the wake should be trailing, as was in fact observed.

Evaluation of the k_y integral in Eq. (3), keeping only the contribution from the pole, then yields

$$\delta\mathbf{v}_i\equiv\delta\dot{\mathbf{r}}_i=-2\,\mathrm{Re}\sum_\alpha\int\frac{dk_x}{4\pi m}\frac{i\hat{\Phi}(\mathbf{k})\mathbf{k}\cdot\hat{e}_\alpha(\mathbf{k})\hat{e}_\alpha(\mathbf{k})}{U-v_{g_y}(\mathbf{k})}\times H\left(\frac{y_0}{U-v_{g_y}(\mathbf{k})}\right)\times e^{ik_xx_0+ik_yy_0+(1/2)[\nu y_0/(U-v_{g_y}(\mathbf{k}))]}\Big|_{k_y=k_{y_0}(k_x)},\tag{6}$$

where $H(x)=(1-\mathrm{sgn}(x))/2$ is a step function, and where $\delta\mathbf{v}_i$ is the perturbed velocity of a dust grain at site i (this is the observable quantity in the experiments). Only solutions of Eq. (5) with $k_{y_0}>0$ are required in Eq. (6). Solutions with $k_{y_0}<0$ are already accounted for by taking twice the real part of the integral, recalling that solutions of Eq. (5) have reflection symmetry through the origin. Also, note that for given k_x there may be more than one positive solution for $k_{y_0}(k_x)$ [see Fig. 4 at small $U/c(0)$, for example]. One must then sum over all such positive solutions in Eq. (6).

For large values of $|x_0|$ or $|y_0|$, the integral in Eq. (6) can be evaluated using the method of stationary phase.[11] At a given location (x_0,y_0) behind the moving charge, the k_x integral is dominated by value(s) of k_x, k_{x_0}, that satisfy $\partial(k_xx_0+k_{y_0}(k_x)y_0)/\partial k_x|_{k_x=k_{x_0}}=0$. This implies the following relation between the opening angle β and the dominant wave number $\mathbf{k}_0$,

$$\tan\beta\equiv\frac{x_0}{-y_0}=\frac{v_{g_x}}{U-v_{g_y}}\Big|_{\mathbf{k}=\mathbf{k}_0},\tag{7}$$

where $\mathbf{k}_0\equiv(k_{x_0},k_{y_0}(k_{x_0}))$. Here we have used Eq. (5) to determine $\partial k_{y_0}/\partial k_x$.

Keeping only the contribution from the compressional mode, and dropping the polarization subscript α, the stationary phase points $\mathbf{k}_0$ yield the following value for the integral in Eq. (6):

$$\delta\mathbf{v}_i=\mathrm{Re}\frac{-i\hat{\Phi}(\mathbf{k}_0)}{m\sqrt{2\pi|y_0u(\mathbf{k}_0)|}}\frac{\mathbf{k}_0\cdot\hat{e}(\mathbf{k}_0)\hat{e}(\mathbf{k}_0)}{U-v_{g_y}(\mathbf{k}_0)}H\left(\frac{y_0}{U-v_{g_y}(\mathbf{k}_0)}\right)\times e^{i\mathbf{k}_0\cdot(x_0,y_0)+(i\pi/4)\,\mathrm{sgn}[y_0u(\mathbf{k}_0)]+(1/2)[\nu y_0/(U-v_{g_y}(\mathbf{k}_0))]},\tag{8}$$

where

$$u(\mathbf{k}_0)\equiv\frac{\partial}{\partial k_x}\left(\frac{v_{g_x}}{U-v_{g_y}}\right)\Big|_{\mathbf{k}=\mathbf{k}_0}.\tag{9}$$

Note that $\mathbf{k}_0=\mathbf{k}_0(\beta)$ through Eq. (7), and that Eq. (8) is valid only where $|y_0u(\mathbf{k}_0)|\gg a^2$.

Equation (8) describes a trailing wake ($y_0<0$) consisting of oscillations that decay like $e^{-\nu|y_0/2(U-v_{g_y})|}/\sqrt{|y_0|}$, with distance $|y_0|$ behind the moving charge. The oscillations have a spatially-varying wave number $\mathbf{k}_0$ that depends on opening angle β through Eq. (7). A graphical solution for $\mathbf{k}_0(\beta)$ can be obtained using Fig. 5 for the case $\lambda/a=1$. The figure displays the right-hand side of Eq. (7) versus k_{x_0} for three different values of the speed U. A given value of β determines one (or more) values of $k_{x_0}(\beta)$, and then $k_{y_0}(\beta)=k_{y_0}(k_{x_0}(\beta))$ through Eq. (5). This value of β defines a line $x_0=-y_0\tan\beta$, along which $\mathbf{k}_0(\beta)$ is the dominant wave number in the wake. Note that the angle of propagation of $\mathbf{k}_0$, θ, is not necessarily the same as β, so wavefronts need not emanate directly from the moving charge as they do in a Mach cone.

Figure 5 shows that, depending on the value of β, there may be no solution, or one or more solutions for $\mathbf{k}_0$. Different solutions at given β correspond to different oscillations

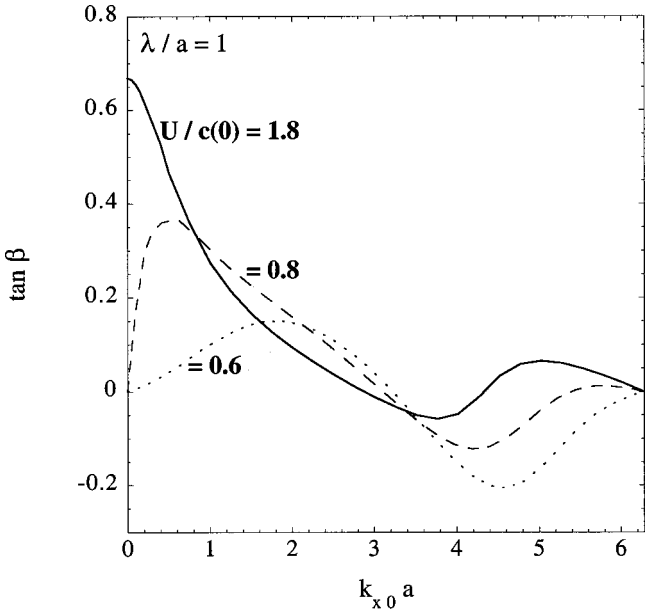

FIG. 5. For a given value of the opening angle β, the curves provide stationary-phase values for the x-component of the wave number, k_{x_0}. $\lambda/a=1$ is assumed.

that are superimposed on one another. Most of these oscillations are at very high wave number, beyond the first Brillouin zone, and hence are of low amplitude since $\hat{\Phi}(\mathbf{k})\to 0$ at large k. However, when $U>c(0)$ there is a single $k_{x_0}(\beta)$ solution at small wave numbers, and this k_{x_0} value approaches zero as β increases towards a maximum.

The maximum β value can be determined by using the long wavelength dispersion relation, $\omega=c(0)k$, in Eqs. (5) and (7). The result is

$$(\tan\beta)_{\max}=\frac{c(0)}{\sqrt{U^2-c(0)^2}},\quad U>c(0). \tag{10}$$

The line $x_0=-y_0(\tan\beta)_{\max}$ defines an opening angle $\beta=\theta_0$ that satisfies the Mach condition, Eq. (1). According to our stationary phase approximation, Eq. (8), there is no wake beyond this opening angle when $U>c(0)$. However, this approximation is not precisely correct, because Eq. (8) breaks down as $k_{x_0}\to 0$, since $u\to 0$ there [see Fig. 5 and Eq. (9)]. The structure of this linear Mach cone can be determined analytically by keeping a slightly more accurate expression for ω, valid at small k,

$$\omega=c(0)k-Ak^3, \tag{11}$$

where $A>0$ for the compressional phonons. (Here we neglect the slight dependence of A on propagation direction in a triangular Yukawa lattice. Examination of the exact dispersion relation using Eq. (4) reveals that $|[A(\theta)-A(0)]/A(0)|<1\%$ for $\lambda/a\gtrsim 1$. This is discussed in more detail in the Appendix.) Equation (5) then implies that

$$k_{y_0}=\tan\theta_0|k_x|\left(1-\frac{Ak_x^2}{c(0)\cos^4\theta_0}\right)+\cdots,\quad k_x a\ll 1, \tag{12}$$

where $U>c(0)$ is assumed, and θ_0 is given by Eq. (1). Noting that the compressional mode has $\hat{e}(\mathbf{k})=\hat{k}$ at long wavelengths, Eq. (6) yields the following expression for the velocity of the wake in the linear Mach cone:

$$\delta\mathbf{v}_{\rm Mach}\simeq \mathrm{Im}\,\hat{\Phi}(0)\frac{e^{(\nu y_0\sin\theta_0/2c(0)\cos^2\theta_0)}\sin\theta_0}{mc(0)\cos^2\theta_0}\times\int_{-\varepsilon}^{\varepsilon}\frac{dk_x}{2\pi}k_x e^{ik_x z+ibk_x^2|k_x|}(1,\mathrm{sgn}(k_x)\tan\theta_0), \tag{13}$$

where $z=x_0+\mathrm{sgn}|k_x|y_0\tan\theta_0$, $b=A\sin\theta_0|y_0|/c(0)\cos^5\theta_0$, and $\varepsilon a\ll 1$ is assumed, as we are interested only in the long wavelengths that contribute in the stationary phase approximation to the linear Mach cone around $z/|y_0|=0$ (i.e., $x\approx\pm y_0\tan\theta_0$). We have used Eq. (1) for θ_0, along with $v_{g_y}\simeq c(0)\sin\theta_0$ (valid for $ka\ll 1$). Assuming that $|y_0|\gg a$ (but that $|z/|y_0|\ll 1$), we can then take $\varepsilon\to\infty$, and the integral can be evaluated analytically, yielding

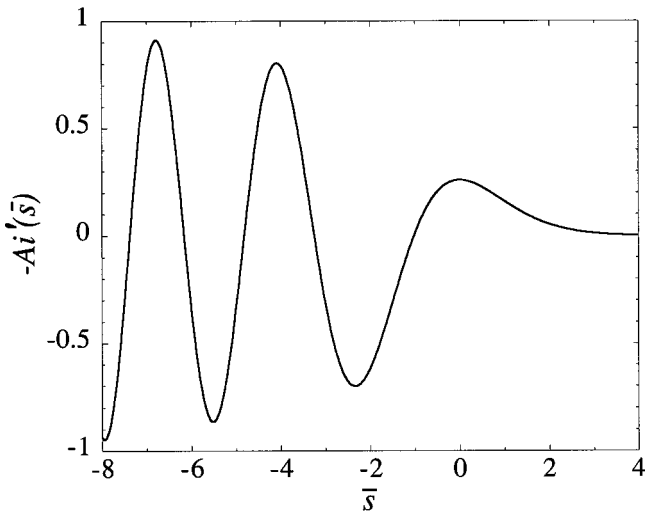

FIG. 6. Functional form of the wake velocity [Eq. (14)] in the linear Mach cone for $U>c(0)$, including the first few oscillations in the lateral wake. Here $\bar{s}$ is a coordinate transverse to the cone, scaled by the distance $(3b)^{1/3}$: $\bar{s}=(|x_0|+y_0\tan\theta_0)/(3b)^{1/3}$.

$$\delta\mathbf{v}_{\rm Mach}=-\frac{\hat{\Phi}(0)\sin\theta_0}{2mc(0)(3b)^{2/3}\cos^3\theta_0}\hat{s}\,A_i'\left(\frac{s}{(3b)^{1/3}}\right)\times e^{(\nu y_0\sin\theta_0/2c(0)\cos^2\theta_0)}, \tag{14}$$

where $s=|x_0|+y_0\tan\theta_0$, $\hat{s}=(\mathrm{sgn}(x_0)\cos\theta_0,\sin\theta_0)$ is a unit vector transverse to the Mach cone, pointing in the forward direction, and $A_i'(x)$ is the derivative of an Airy function. Note that $\hat{\Phi}(0)=\int d^2r\Phi(\mathbf{r})$ is a real number. Equation (14) is only valid near the Mach cone, for $|s/y_0|\ll 1$. The form of the wake is displayed in Fig. 6, assuming no damping ($\nu=0$). One can see that the wake decays exponentially in the forward direction (s increasing) and oscillates toward the rear ($s<0$). Each crest in the oscillation corresponds to a line in Fig. 2(a). The distance between crests has a scale length of $(3b)^{1/3}$, and this scale length is small compared to $|y_0|$ for $|y_0|$ large. Therefore, several oscillations in the lateral wake are described by Eq. (14), provided that one looks well behind the moving charge.

One can easily show that $\delta\mathbf{v}_{\rm Mach}\cdot\hat{s}$ has an extremum at $s=0$, and the extremum value is

$$(\delta\mathbf{v}_{\rm Mach}\cdot\hat{s})_{\rm ext}=\frac{\hat{\Phi}(0)}{6\Gamma(1/3)\,mc(0)^{1/3}}\frac{(\sin\theta_0\cos\theta_0)^{1/3}}{(4A|y_0|)^{2/3}}\times e^{(\nu y_0\sin\theta_0/2c(0)\cos^2\theta_0)}, \tag{15}$$

where $\Gamma(x)$ is a gamma function. Therefore, the direction of $\delta\mathbf{v}_{\rm Mach}$ at the extremum depends on the sign of $\hat{\Phi}(0)$. For $\hat{\Phi}(0)>0$, $\delta\mathbf{v}_{\rm Mach}$ points *forward* [along $(\cos\theta_0,\sin\theta_0)$ for $x_0=-y_0\tan\theta_0$, or along $(-\cos\theta_0,\sin\theta_0)$ for $x_0=y_0\tan\theta_0$], but for $\hat{\Phi}(0)<0$, $\delta\mathbf{v}_{\rm Mach}$ points *backward*. In the experiments, $\delta\mathbf{v}_{\rm Mach}$ pointed forward, implying $\hat{\Phi}(0)>0$.

If one assumes that $\Phi(r)$ is either purely attractive or purely repulsive, then it is easy to see that $\hat{\Phi}(0)>0$ implies

a repulsive potential and $\hat{\Phi}(0)<0$ implies an attractive potential. For instance, for a purely repulsive potential the derivative of $\Phi(r)$ with respect to r is negative at all $r>0$, and $\Phi(r)$ is zero at infinity. This necessarily implies that the radial average of $\Phi(r)$ is greater than zero. Thus, the fact that $\delta\mathbf{v}_{\rm mach}$ pointed forward in the experiments implies that the force between the moving charge and the dust grains cannot be purely attractive; the force must have a significant repulsive component, and may even be purely repulsive.

In the experiments and simulations of Refs. 1 and 2, the wake velocity reversed direction in each successive ''Mach cone'' as one counted back from the initial Mach cone. This is consistent with the oscillatory form of the wake, as shown in Figs. 2 and 6. [Note that in Fig. 2, locations of the wave crests are drawn, assuming a repulsive interaction between the grains and the moving charge. There are also troughs (not shown) between the crests where the wake velocity reverses direction.]

Summarizing the results so far, for $U>c(0)$ there is a linear Mach cone with an extremum in $\delta\mathbf{v}\cdot\hat{s}$ along the lines $x_0=\mp y_0\tan\theta_0$, together with a set of oscillations behind the cone, determined by the exponential in Eq. (8). Assuming that $\hat{\Phi}(\mathbf{k})$ is real for all $\mathbf{k}$, the oscillations are proportional to $\sin[\mathbf{k}_0\cdot(x_0,y_0)+(\pi/4)\,\mathrm{sgn}(y_0u(\mathbf{k}_0))]$. The peaks (maxima) in this function are shown in Fig. 2(a), along with the Mach cone maximum, for the case $\nu=0$ (no damping), $U/c(0)=1.8$, and $\lambda/a=1$ in the Yukawa potential.

The oscillation at relatively large opening angles behind the Mach cone is termed a ''lateral wake,'' in analogy to the similar structure behind a moving ship.[4] The complex set of criss-crossing extrema directly behind the moving charge are superimposed on the slower-varying lateral wake. They are a result of the large-wave number umklapp phonon solutions for $k_{x_0}(\beta)$. The extent to which these solutions actually affect the wake depends on the magnitude of $\hat{\Phi}(\mathbf{k})$ at large $\mathbf{k}$. For example, if $\hat{\Phi}(\mathbf{k})$ were zero for wave numbers beyond the first Brillouin zone, only the lateral wake and the Mach cone would appear.

Note that the wavefronts in the lateral wake curve outward until they are parallel to the Mach cone at large distances behind the moving charge. However, if finite damping ν is added to the solution, these wavefronts decay exponentially before they achieve the same opening angle as the Mach cone. The experiments and simulations, which had finite damping, also observed that the secondary wavefronts had smaller opening angles than the Mach cone.[1,2]

We now turn to the case where the grain moves with speed $U<c(0)$, a case which has not yet been reported in the experiments. In this regime there is no longer a solution to Eq. (1), and consequently the Mach cone disappears [see also Eq. (15) in the limit $\cos\theta_0\to 0$]. Now a new small-wave-number solution for $k_{x_0}(\beta)$ appears, corresponding to a transverse wake that is superimposed on the lateral wake (see Fig. 5). The appearance of the transverse wake can be understood analytically when $0\leqslant c(0)/U-1\ll 1$. In this regime, the transverse wake has wave numbers $k_0\ll a^{-1}$, so Eq. (11) holds. Then Eqs. (7) and (11) can be combined to give

$$\tan\beta=\frac{v_g\sqrt{1-c^2/U^2}}{U-v_gc/U}, \tag{16}$$

where $v_g=c(0)-3Ak^2$ is the magnitude of the group velocity, and $c=c(k)=c(0)-Ak^2$ is the magnitude of the phase velocity. We may now regard the opening angle β as a function of k. This function is double-valued at small k; there are two values of k for every β, indicating two wakes. This is because a maximum in $\beta(k)$ exists, at $k_{\rm max}=\sqrt{3(c(0)-U)/2A}$, for $c(0)/U-1$ small (but positive). The range $k>k_{\rm max}$ corresponds to the lateral wake, but $k<k_{\rm max}$ corresponds to the new transverse wake. This wake also has k bounded from below, $k\geqslant k_{\rm min}$, where $k_{\rm min}=\sqrt{(c(0)-U)/A}$, in order that $c(k)^2/U^2\leqslant 1$. At $k=k_{\rm min}$, $\tan\beta=0$, so $k=k_{\rm min}$ corresponds to the wave number of the transverse wake on a line directly behind the moving charge. The wave number $k=k_{\rm max}$ corresponds to the maximum value of β, beyond which there is no wake. For small but positive $c(0)/U-1$, Eq. (16) implies

$$(\tan\beta)_{\rm max}=\frac{1}{4\sqrt{c(0)/U-1}}. \tag{17}$$

This shows that as U increases and approaches $c(0)$ from below, $\beta\to\pi/2$ and the wake opens up until it fills the entire half-plane behind the charge. As U increases further, Eq. (10) becomes valid and the wake beings to narrow again.

At $k=k_{\rm max}$, the transverse and lateral wakes meet. At this point $u(\mathbf{k}_0)=0$, Eq. (8) breaks down, and the amplitude of the wake is large. One can show that $u>0$ for the transverse wake and $u<0$ for the lateral wake (see Fig. 5), so according to Eq. (8) there is a 1/4 period phase shift between the two wakes. The resulting structure is shown in Fig. 2(b) for the same parameters as Fig. 2(a), except now $U/c(0)=0.8$. As before, the figure shows the maxima of $\sin[\mathbf{k}_0\cdot(x_0,y_0)+\pi/4\,\mathrm{sgn}(y_0u(\mathbf{k}_0))]$. In addition to the transverse and lateral wakes, there is a narrow band of umklapp phonons caused by high wave number components of $\Phi(\mathbf{k})$, similar to that in Fig. 2(a). As $U/c(0)$ decreases further, this band increases in width as the lateral wake decreases in width, and eventually these umklapp phonons dominate the wake structure.

III. DISCUSSION

We have shown that the wake of compressional phonons excited in a 2D crystal lattice by a moving charge has a structure which depends on two dimensionless parameters: the ratio of the speed U of the charge compared to the phase speed of long wavelength phonons, $c(0)$; and the ratio of the Debye screening length λ in the intergrain interaction to the spacing between dust grains, a. When $U/c(0)>1$, a linear Mach cone and lateral wake form, along with a series of relatively high wave number structures directly behind the charge [see Fig. 2(a)]. This type of wake is qualitatively similar to that observed in recent experiments on 2D plasma crystals. When $U/c(0)<1$, the Mach cone is predicted to disappear, to be replaced by a transverse wake [Fig. 2(b)]. This type of wake has not yet been observed.

The structure of the wake also depends on the interaction between the dust grains and the moving charge. The form of this interaction is presently the subject of debate.[5–9] Our theory analysis of the wakes observed in Refs. 1 and 2 implies that the interaction between the grains and the moving charge cannot be purely attractive; the force either changes sign or is purely repulsive. The fact that the spatial average of the effective interaction potential is positive $[\hat{\Phi}(0)>0]$ implies that there must be a *substantial* repulsive component to the force. This could be accomplished in several ways: through a purely repulsive force, or a repulsive tail at large radial displacements, or a strong short-range repulsion, for example.

The dependence of the wake structure on λ/a can be understood from Eq. (14), when $U>c(0)$. The scale length of the wake appearing in this equation, $(3b)^{1/3}$, depends implicitly on λ/a through A and $c(0)$. For fixed $U/c(0)>1$, the scale length increases as λ/a, increases, varying roughly as $(\lambda/a)^{2/3}$ when $\lambda/a>1$. [This follows from the mean field forms of $c(0)$ and A, Eqs. (A6) and (A9).] Since the form of the wake depends on both λ/a and $U/c(0)$, and since $c(0)$ depends on the charge Q on the dust grains, experimental measurement of the wake structure could be used to determine both Q and λ, independent from other measurement techniques.

A particularly striking example of the dependence of the wake on the Debye length is the case of a purely Coulombic interaction with $\lambda=\infty$. In this limit, long wavelength compressional phonons have infinite phase speed in a 2D lattice [i.e., $c(0)\to\infty$ (Ref. 12)] (see the Appendix). Thus, for a Coulomb interaction between the charges no Mach cone should be formed, even for very large U, and the wake should be of the type shown in Fig. 2(b).

While the limit of a pure Coulomb interaction is difficult to achieve in dust-plasma experiments due to the shielding effect of the background plasma, 2D lattices interacting via a Coulomb force have been created in Penning traps.[13] It may be possible to excite a wake in such a 2D Coulomb crystal, perhaps by using a laser spot moving with respect to the lattice, as discussed in Ref. 2. However, the strong imposed magnetic field in a Penning trap would affect the form of the wake, and the theory for this physical situation remains to be worked out.

The theory presented here has assumed linear dynamics for the dust grains. While this approximation appears to be sufficient to explain qualitative aspects of the wake structure, nonlinear effects could play an important role if the interaction Φ between the moving charge and the grains is sufficiently strong. One might then expect that an elastic shock could form, similar to those that have been studied in solid materials.[14] This possibility will be the subject of future work.

The theory presented here also assumes that the moving charge has constant velocity. In fact, the wake itself carries momentum away, creating a drag force on the charge. Since the charge in the experiment is observed to move at nearly constant speed, presumably some external force is acting in the experiments to counteract the effects of the wake drag as well as drag due to neutral gas. The drag from the phonon wake is the condensed-matter equivalent of the drag due to inverse-Landau-damping in a collisionless plasma,[15] or the ''wave resistance'' on a moving ship.[16] The magnitude of this drag force, together with its dependence on velocity and the particle interaction, will be the subject of future work.

ACKNOWLEDGMENTS

This work was completed with the support of National Science Foundation Grant No. PHY-9876999 and Office of Naval Research Grant No. N00014-96-1-0239.

APPENDIX: THE COMPRESSIONAL PHONONS IN A 2D TRIANGULAR YUKAWA LATTICE

In this Appendix we derive several results regarding the frequency $\omega(\mathbf{k})$ for the compressional mode of a 2D triangular lattice of charges that interact via a Yukawa potential $\phi(\mathbf{r})$. First, we consider the phase speed of long-wavelength compressional phonons, $c(0)$. A general expression for $c(0)$ can be obtained from the matrix $\mathbf{M}(\mathbf{k})$ in the limit as $\mathbf{k}\to 0$. We first note that for any central potential $\phi(r)$, Eq. (4) implies that $\mathbf{M}(\mathbf{k})$ can be written as

$$\mathbf{M}(\mathbf{k})=\frac{1}{m}\sum_{\mathbf{p}}\left[\frac{\mathbf{pp}}{p^2}\left(\frac{\partial^2\phi}{\partial p^2}-\frac{1}{p}\frac{\partial\phi}{\partial p}\right)+\frac{\mathbf{1}}{p}\frac{\partial\phi}{\partial p}\right][1-\cos\mathbf{k}\cdot\mathbf{p}], \tag{A1}$$

where $\mathbf{p}=\mathbf{r}_j-\mathbf{r}_i$ is a lattice vector, $\mathbf{1}$ is the unit tensor, and the sum runs over all $\mathbf{p}\neq 0$. Taylor expanding Eq. (A1), and using the fact that compressional phonons have polarization $\hat{e}\|\mathbf{k}$ at small wave number, we have

$$c^2(0)=\frac{1}{2m}\sum_{\mathbf{p}}\left[\frac{p_x^2}{p^2}\frac{\partial^2\phi}{\partial p^2}+\frac{p_y^2}{p^3}\frac{\partial\phi}{\partial p}\right]p_x^2. \tag{A2}$$

This phase speed is shown in Fig. 7 as a function of the Debye length scaled to the interparticle spacing, λ/a.

Several analytic or semianalytic approximations to $c(0)$ [and $\omega(k)$] can also be obtained. For example, one can keep only nearest-neighbor interactions in Eq. (A2), which is a reasonable approximation provided that $\lambda/a\ll 1$.[1] In this case Eq. (A2) reduces to

$$c_{nn}(0)^2=\left[15\left(1+\frac{a}{\lambda}\right)+\frac{9a^2}{\lambda^2}\right]\frac{Q^2}{8ma}e^{-a/\lambda}. \tag{A3}$$

Comparison of Eq. (A3) to the exact result in Fig. 7 shows that Eq. (A3) works well provided $\lambda/a\lesssim 0.3$.

A second analytic approximation can be found using a ''mean-field'' approach. In this approach one entirely neglects the triangular lattice structure and replaces the $\Sigma_{\mathbf{p}}$ in Eq. (A1) by an integral, $n_D\int d^2r$, noting that the integral is convergent as $r\to 0$. Here n_D is the density per unit area of the dust. The resulting matrix is diagonal with a compressional phonon frequency given by the expression

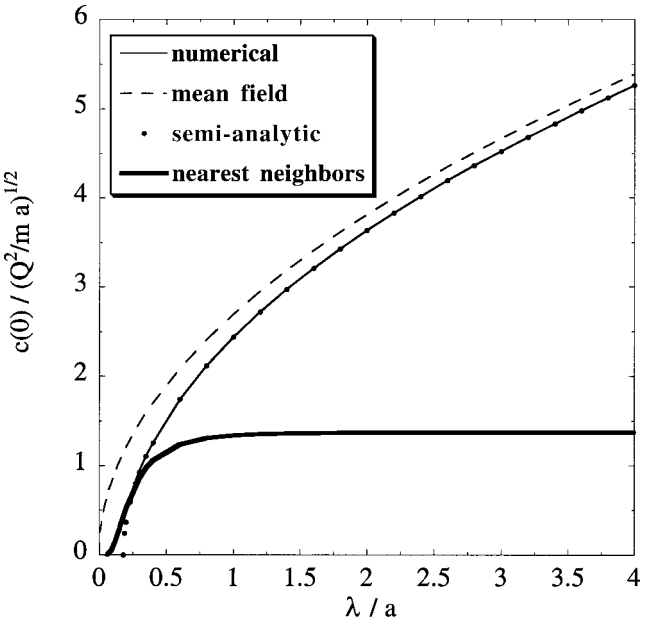

FIG. 7. Phase speed for compressional modes at $\mathbf{k}=0$ versus λ/a in the Yukawa potential. Thin solid line, numerically determined via Eq. (A2). Dashed line, mean field theory [Eq. (A6)]. Dots, semianalytic [Eq. (A7)]. Thick solid line, nearest-neighbor interactions [Eq. (A3)].

$$\omega_{\mathrm{MF}}^2(k)=\frac{n_D}{m}\int_0^{2\pi}d\theta\int_0^{\infty}rdr(1-\cos(kr\cos\theta))\times\left[\cos^2\theta\frac{\partial^2\phi}{\partial r^2}+\frac{\sin^2\theta}{r}\frac{\partial\phi}{\partial r}\right]. \tag{A4}$$

For a Yukawa potential these integrals can be performed analytically, yielding

$$\omega_{\mathrm{MF}}^2(k)=\frac{2\pi Q^2 n_D}{m}\frac{k^2\lambda}{\sqrt{1+k^2\lambda^2}}. \tag{A5}$$

The long-wavelength limit of this expression yields a mean-field result for $c(0)$, $c_{\mathrm{MF}}(0)$,

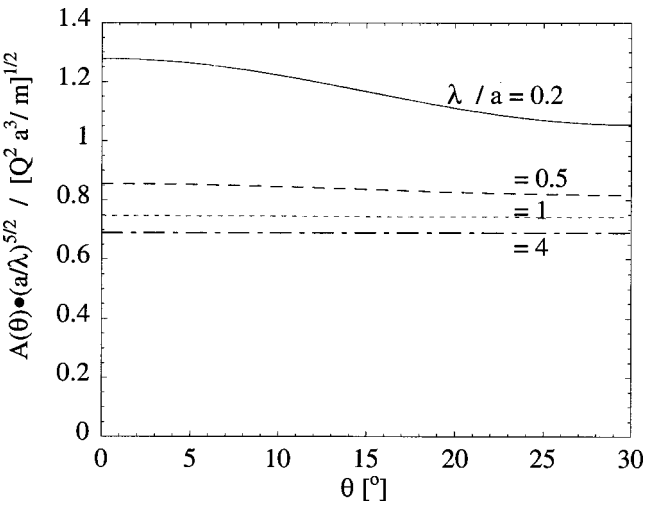

FIG. 8. Variation of cubic term A with angle of propagation θ for 4 values of λ/a. A is divided by $\lambda^{5/2}$ so that data are all on the same scale.

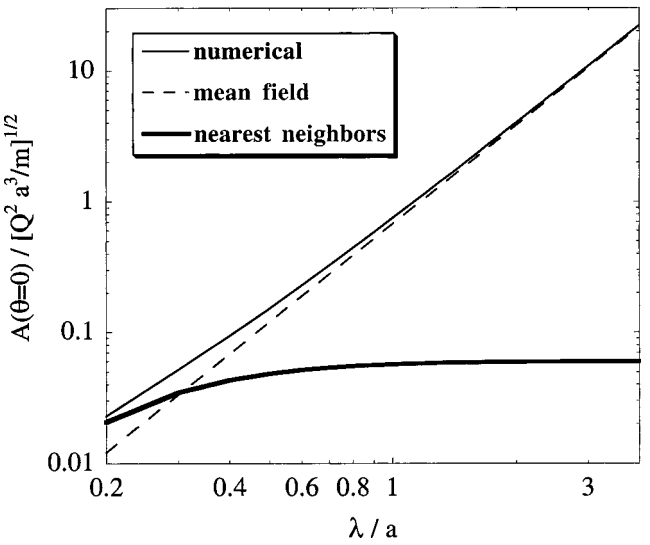

FIG. 9. Variation of $A(\theta=0)$ with λ/a. Thin solid line, numerically determined via Eq. (A11). Dashed line, mean field theory [Eq. (A9)]. Thick solid line, theory using nearest-neighbor interactions [Eq. (A12)].

$$c_{\mathrm{MF}}^2(0)=\frac{2\pi Q^2\lambda n_D}{m}. \tag{A6}$$

Comparing to the exact result in Fig. 7 shows that $c_{\mathrm{MF}}(0)$ works reasonably well except for a positive offset. This is caused by the effect of nearby particles (small r) in the integral in Eq. (A4). A semianalytic approximation that works well for $\lambda/a\gtrsim 0.3$ is

$$c_{\mathrm{SA}}^2(0)=c_{\mathrm{MF}}^2(0)-1.32\left(\frac{Q^2}{ma}\right). \tag{A7}$$

Note that for $\lambda\to\infty$, $c_{\mathrm{MF}}^2(0)\to\infty$. In fact, Eq. (A5) shows that in this limit (the limit of a pure Coulombic interaction), the mean-field dispersion relation is[12]

$$\lim_{\lambda\to\infty}\omega_{\mathrm{MF}}^2(k)=\frac{2\pi Q^2 n_D k}{m}. \tag{A8}$$

This dispersion relation is identical to that for deep water surface gravity waves, $\omega^2=gk$, with $2\pi Q^2 n_D/m$ taking the role of the acceleration of gravity g. Therefore, the long-wavelength features of the wake in a 2D Coulomb crystal should strongly resemble the Kelvin wedge behind a moving ship in deep water.

Finally, we note that several of our results, such as the functional form of the Mach cone, depend on the cubic term in the dispersion relation, $-Ak^3$ [see Eq. (11)]. An analytic approximation to A can be obtained in the mean-field approximation from Eq. (A5),

$$A_{\mathrm{MF}}=\frac{1}{2}\lambda^{5/2}\left(\frac{\pi Q^2 n_D}{2m}\right)^{1/2}. \tag{A9}$$

In a triangular lattice A actually varies slightly with propagation direction. This slight variation is shown for a few cases in Fig. 8. Here we have evaluated $A(\theta)$ using the exact

dispersion relation obtained from Eq. (4). This involves Taylor expanding Eq. (4) to fourth-order in k. The fourth order correction to the matrix is

$$\Delta\mathbf{M}=-\frac{1}{24m}\sum_{j\neq i}\frac{\partial^2\phi}{\partial\mathbf{r}_i\partial\mathbf{r}_i}(\mathbf{r}_i-\mathbf{r}_j)[\mathbf{k}\cdot(\mathbf{r}_i-\mathbf{r}_j)]^4. \tag{A10}$$

Then a standard first-order perturbation theory treatment yields the following result for $A(\theta)$:

$$A(\theta)=-\frac{\hat{k}\cdot\Delta\mathbf{M}\cdot\hat{k}}{2c(0)k^4}. \tag{A11}$$

In the limit of small λ/a, keeping only nearest-neighbor interactions in Eq. (A10) yields

$$A(\theta)=\frac{a^3Q^2}{256\lambda^2c_{nn}(0)}e^{-a/\lambda}\left[10+\cos 6\theta+3(6+\cos 6\theta)\times\left(\frac{\lambda}{a}+\frac{\lambda^2}{a^2}\right)\right],\quad \frac{\lambda}{a}\ll 1 \tag{A12}$$

showing that even at small λ/a there is at most a 20% variation in A with angle of propagation. Since the variation in $A(\theta)$ is small for $\lambda/a\gtrsim 1$, we compare Eq. (A9) to $A(0)$ as a function of λ/a in Fig. 9. The mean field approximation is reasonably accurate, except at small λ/a where Eq. (A12) works well.

[1] D. Samsonov, J. Goree, Z. W. Ma, and A. Bhattacharjee, Phys. Rev. Lett. **83**, 3649 (1999).
[2] D. Samsonov, J. Goree, H. M. Thomas, and G. E. Morfill, Phys. Rev. E **61**, 5557 (2000).
[3] See, for example, Yoshi-Hiko Oktsuki, *Charged Beam Interaction with Solids* (Taylor and Francis, New York, 1983), p. 63.
[4] W. Thomson (Lord Kelvin), ''On Ship Waves,'' Proc. Inst. Mech. Eng., 1887 [Popular lectures, iii. 482]; H. Lamb, *Hydrodynamics* (Dover, New York, 1985), p. 434.
[5] U. Konopka, G. E. Morfill, and L. Ratke, Phys. Rev. Lett. **84**, 891 (2000).
[6] A. Melzer, V. A. Shweigert, and A. Piel, Phys. Rev. Lett. **83**, 3194 (1999).
[7] J. H. Chu and I. Lin, Phys. Rev. Lett. **72**, 4009 (1994).
[8] S. Vladimirov and M. Nambu, Phys. Rev. E **52**, 2172 (1995).
[9] F. Melandsø and J. Goree, Phys. Rev. E **52**, 5312 (1995).
[10] F. M. Peeters and X. Wu, Phys. Rev. A **35**, 3109 (1987).
[11] C. M. Bender and S. A. Orzag, *Advanced Mathematical Methods for Scientists and Engineers* (McGraw–Hill, New York, 1978), p. 276.
[12] K. I. Golden, G. Kalman, and P. Wyns, Phys. Rev. A **41**, 6940 (1990).
[13] T. B. Mitchell, J. J. Bollinger, D. H. E. Dubin, X.-P. Huang, W. M. Itano, and R. H. Baughman, Science **282**, 1290 (1998).
[14] R. Courant and K. Friedrichs, *Supersonic Flows and Shock Waves* (Springer-Verlag, New York, 1948), p. 235.
[15] S. Ichimaru, *Basic Principles of Plasma Physics* (Benjamin, Reading, 1973), p. 67.
[16] H. Lamb, in Ref. 4, p. 413.